The Role of Conformational Dynamics in Abacavir-Induced Hypersensitivity Syndrome

Itamar Kass[1*], James Fodor[1], Blake T. Riley[1], Ashley M. Buckle[1,#], Natalie A. Borg[1,#]

[1]Department of Biochemistry and Molecular Biology, Biomedicine Discovery Institute, Monash University, Clayton, Victoria, Australia 3800

[#]Joint senior authors and to whom correspondence should be addressed

Natalie A. Borg, PhD.
Department of Biochemistry and Molecular Biology,
Biomedicine Discovery Institute,
Monash University, Clayton, 3800, Victoria, Australia.
E-mail: natalie.borg@monash.edu, Tel: +613-9902-9369, Fax: +613-9905-5645

Ashley M. Buckle, PhD.
Department of Biochemistry and Molecular Biology,
Biomedicine Discovery Institute,
Monash University, Clayton, 3800, Victoria, Australia.
E-mail: ashley.buckle@monash.edu, Tel: +613-9902-9313, Fax: +613-9905-5645

Keywords: MHC | TCR | conformational dynamics | molecular dynamics | HIV | drug hypersensitivity

Running Title: Dynamics in abacavir hypersensitivity

Abstract

We have analyzed the dynamics of three different peptides bound to HLA-B*57:01 with and without abacavir, an antiretroviral drug used mainly to treat acquired immune deficiency syndrome (AIDS) caused by human immunodeficiency virus (HIV) type 1. Abacavir is associated with drug hypersensitivity reactions in 2% to 8% of treated patients. This hypersensitivity is strongly associated with human leukocyte antigen (HLA)-B*57:01 positive patients, but not patients carrying closely related alleles HLA-B*57:03, HLA-B*57:02 and HLA-B*58:01. Using molecular dynamics (MD) we found that abacavir alters the conformations adopted by peptides bound to HLA-B*57:01, as well as reducing their flexibility. The presence of abacavir has a direct impact on the dynamics and the conformational space available to peptides bound to HLA-B*57:01, likely influencing abacavir-induced immune self-reactivity. Abacavir binds dynamically, forming variable interactions with HLA-B*57:01 that are not accessible from static crystallographic snapshots, and may explain its specificity to HLA-B*57:01. The main contribution of abacavir to complex stability is through its effect on the shape of the binding groove, rather than through direct interactions with binding pockets. Understanding how dynamics influences the interactions of abacavir with HLA-B*57:01 and bound peptides will be important for developing safer antiretroviral drugs for the treatment and prevention of HIV.

Introduction

Abacavir is an antiretroviral medication used for the treatment of HIV/AIDS [1, 2]. It is a prodrug that is converted by the liver [3] to form the pharmacologically active compound carbovir 5′-triphosphate [4], an analogue of guanosine that targets HIV reverse transcriptase. Abacavir has been found to elicit a drug hypersensitivity reaction (DHR) in 2% to 8% of treated patients [5], with hypersensitivity attributed to the prodrug itself [6, 7]. Symptoms of abacavir hypersensitivity syndrome (AHS) include fever, malaise, nausea, diarrhoea and skin rash, and the condition can be fatal in severe cases [8]. AHS is strongly associated with the presence of the human leukocyte antigen HLA-B*57:01 allele, and is mediated by the activation of HLA-B*57:01 restricted CD8+ T-cells [9-11]. In contrast, no hypersensitivity reaction is observed in patients carrying the closely related alleles HLA-B*57:03, HLA-B*57:02, or HLA-B*58:01 [6, 10].

Crystal structures of HLA-B*57:01-peptide-abacavir complexes reveal abacavir binds non-covalently at the floor of the peptide-binding cleft, and makes contacts with F-pocket residues that differ in HLA-B*57:03, HLA-B*57:02 and HLA-B*58:01 [6, 7]. It has therefore been suggested that abacavir changes the chemistry and shape of the peptide binding cleft, thereby altering the repertoire of peptides that can be presented by HLA-B*57:01. These insights notwithstanding, the structures of the HLA-B*57:01-abacavir-peptide complex are insufficient to account for the molecular basis of AHS. Specifically, a comparison of HLA-B*57:01-peptide structures both with abacavir (PDB codes 5U98 [12], 3UPR [7], 3VRI and 3VRJ [6]) and without (PDB codes 2RFX [10]), indicates that both the peptide and abacavir can adopt a range of conformations in the binding cleft. This suggests that conformational dynamics may play an important role in the recognition of HLA-B*57:01 by abacavir-specific T cell receptors (TCRs). The intricacy of the short- and long-lived interactions between the TCR and HLA-B*57:01-peptide is consistent with the role of conformational dynamics in the activation of the immune system [13-17].

In order to better understand the nature of these conformational dynamics and interactions between HLA-B*57:01, bound peptide, and abacavir, we performed a series of MD simulations of three HLA-B*57:01-peptide complexes (hereby referred to as major histocompatibility complex (MHC)-peptide, pMHC complexes) in the presence and absence of abacavir.

Results and Discussion

Abacavir does not affect HLA-B*57:01-peptide stability during simulations

The stability of all HLA-B*57:01-peptide structures throughout the simulations was investigated by computing the root-mean-square deviation (RMSD) of the backbone atoms of each complex, using the original structure coordinates as reference points (Figure S1). RMSD values for all simulated systems reached a plateau after 30 to 50 ns, indicating that all systems reached equilibrium. Relatively small average RMSD values indicate little overall deviation from the original structure during the simulation. The similarity of RMSD values in corresponding systems with and without abacavir indicates that the absence of abacavir does not affect the stability of the system.

Abacavir reduces the flexibility of HLA-B*57:01-bound peptides

While all simulated complexes were found to be stable, the presence of abacavir does affect the dynamics of HLA-B*57:01 and each of the three bound peptides (pep-V, RVAQ, LTTK). Comparison of the root-mean-square fluctuations (RMSF) within the MHC binding cleft (residues 1-180) reveals only minor differences between peptide-bound HLA-B*57:01 with and without abacavir (Figure 1). Whereas the presence of abacavir does not affect the flexibility of the α1 and α2 helices that flank the cleft of HLA-B*57:01, its absence greatly increases the flexibility of the bound peptides. Furthermore, snapshots taken throughout the simulations show that the bound peptides behave differently depending on whether abacavir is present (Figure 2).

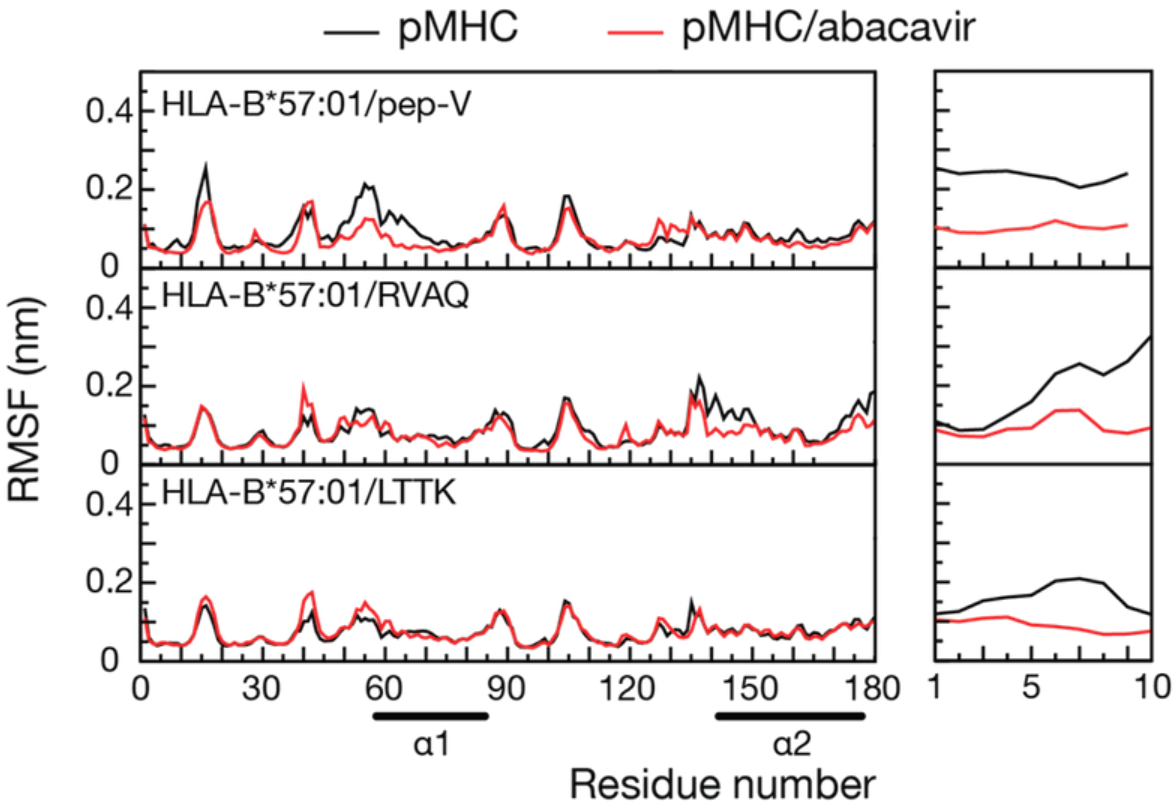

Figure 1. Abacavir reduces the flexibility of HLA-B*57:01-bound peptides. Representative RMSFs calculated from the last 200 ns of each system for MHC heavy chain (left) and bound peptide residues (right). Only positions that define the MHC antigen-binding cleft (residues 1 to 180) are displayed with the MHC α-helices underlined. Simulations without abacavir are in black and with abacavir are in red.

A comparison of all three simulated systems indicates that the stabilizing effect of abacavir is the largest for the 9-mer peptide (pep-V) bound to HLA-B*57:01. In the absence of abacavir, the flexibility of the pep-V peptide backbone is dramatically increased, with neither the N- nor C-termini remaining anchored in their usual pockets (A and F respectively), and consistent with the observation that abacavir is present for pep-V to bind HLA-B*57:01 [7]. The flexibility of the 10-mer peptides (RVAQ and LTTK) bound to HLA-B*57:01 is similarly increased in the absence of abacavir, with the C-terminus likewise not being fixed in the F-pocket, though in this case the N-terminus does remain fixed in the A-pocket (Figure 1). Taken together, these observations suggest that such complexes are not stable without abacavir, and would dissociate over timescales not accessible in this study. This provides a plausible explanation for the lack of experimental evidence of such pMHC complexes in the absence of abacavir [6, 7].

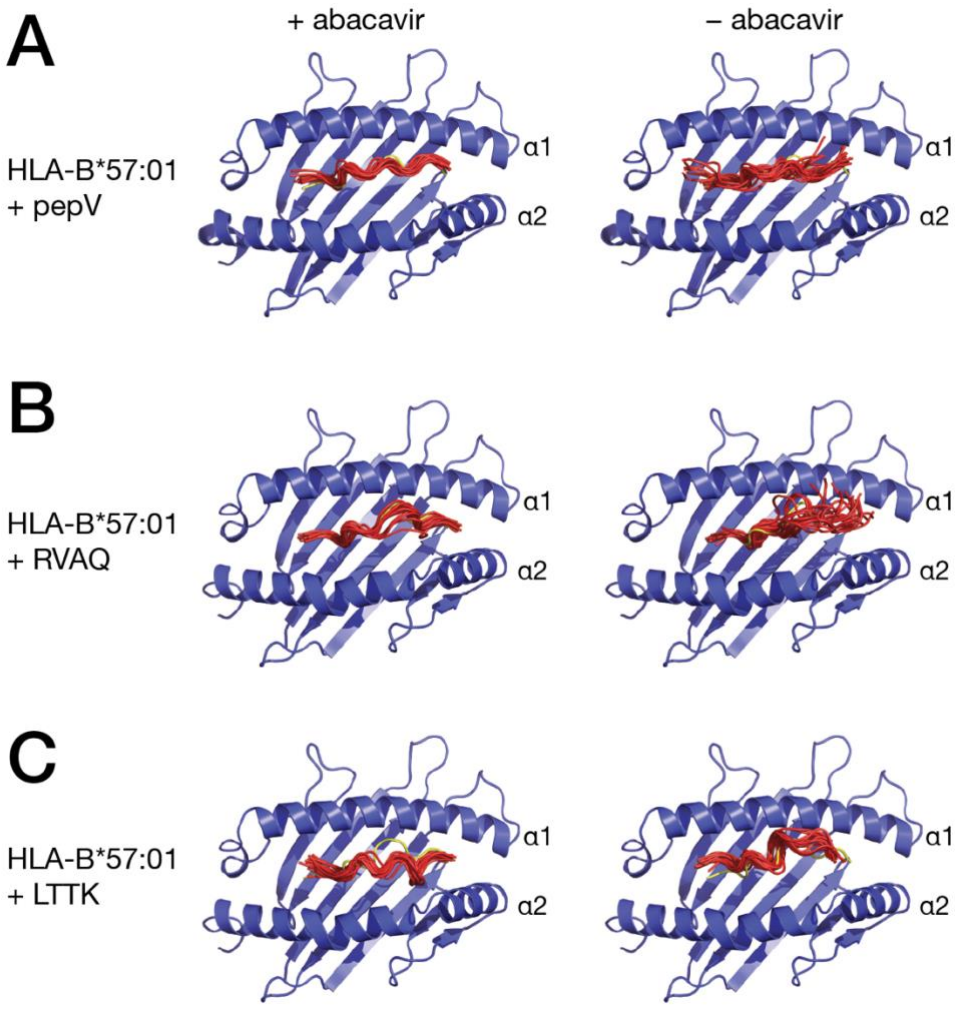

Figure 2. Peptide dynamics is dependent on the presence of abacavir. Bound peptide backbone fluctuations from MD simulations of HLA-B*57:01 **(A)** with pep-V, **(B)** RVAQ and **(C)** LTTK with (left) and without (right) abacavir, indicating the reduced flexibility of the peptide when abacavir is present. Residues 1 to 180 of the pMHC backbone shown as cartoon in blue. Peptide backbone, depicted as ribbon, and colored in yellow (crystal structure conformation) and red (conformations during simulation) are shown as a superposition of 20 structures sampled every 10 ns from the last 200 ns of representative 250 ns simulations.

pMHC interactions are dynamic and are affected by abacavir

Notwithstanding the static picture presented by the crystallographic structures of HLA-B*57:01-peptide-abacavir complexes, our simulations indicate that the complexes are in a state of constant conformational flux. A detailed examination of the pMHC interface over the course of the simulations reveals differences in hydrogen bond (H-bond) occupancy (the fraction of

time that a H-bond bond is formed throughout the simulations) between systems with and without abacavir (Tables S1-S2). While H-bonds between bound peptide and HLA-B*57:01 not seen in the original structures are formed in all the complexes, these additional H-bonds are more abundant in the presence of abacavir than in its absence. Moreover, H-bonds formed in the presence of abacavir show higher occupancies during simulations than those observed in its absence. This indicates that in the presence of abacavir, the peptide is bound relatively tightly in the binding pocket. In addition, the majority of the newly-formed H-bonds are located in the A- and F- pockets. As a result, the presence of abacavir not only stabilizes the binding of peptides to HLA-B*57:01, but also stabilizes specific conformations of the bound peptides. Moreover, while abacavir is capable of forming H-bonds with HLA-B*57:01, our results suggest that even when abacavir is present, the majority of H-bonds still form between HLA-B*57:01 and the bound peptides. This indicates that the main contribution of abacavir to complex stability is through its effect on the shape of the binding groove, rather than through direct interactions with binding pockets.

Fluctuations of bound abacavir

On the basis of our results, we hypothesized that, like the bound peptide, abacavir itself will also exhibit some degree of conformational flexibility, and that such movement is likely to be important for determining its specificity to HLA-B*57:01. Examination of snapshots taken throughout simulations of abacavir in the HLA-B*57:01 binding groove show that abacavir can bind to HLA-B*57:01 in many similar but distinct conformations, and this range of conformations are likely obstructed by closely related alleles harbouring bulkier amino acids (Figure 3). Furthermore, during simulations new H-bonds not seen in the static crystallographic structure are formed, which are capable of stabilizing the new conformations of the HLA-B*57:01-peptide-abacavir complex (Figure S2).

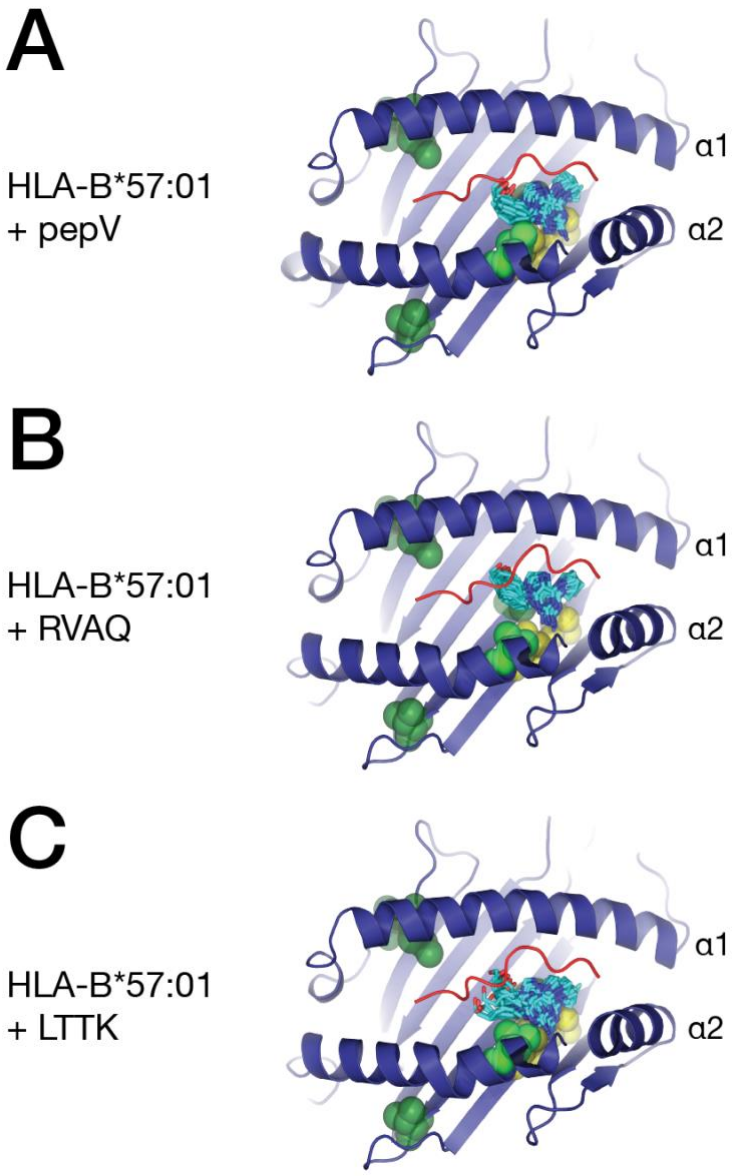

Figure 3. A comparison of abacavir dynamics during all-atom MD simulations of HLA-B*57:01-peptide-abacavir. Abacavir fluctuations from MD simulations of HLA-B*57:01 with **(A)** pep-V, **(B)** RVAQ and **(C)** LTTK. Abacavir heavy atoms (drawn as stick and shown in CPK coloring) are shown as a superposition of 20 structures sampled every 10 ns from the last 200 ns of representative 250 ns simulations. Residues which differ between HLA-B*57:01, which is associated with abacavir hypersensitivity syndrome, and closely related alleles for which there is no associated hypersensitivity including HLA-B*57:03 (Asp114Asn; Ser116Tyr), HLA-B*57:02 (Asp114Asn; Ser116Tyr; Leu156Arg), and HLA-B*58:01 (Met45Thr; Ala46Glu; Val97Arg; Val103Leu) are grouped into sets and drawn as transparent spheres coloured yellow (Asp114 and Ser116), light green (Leu156) and dark green (Met45,

Ala46, Val97 and Val103). Residues 1 to 180 of the MHC backbone starting structure (represented as blue cartoon) are drawn for clarity.

Our observation that abacavir retains some flexibility while lodged between HLA-B*57:01 and the bound peptide implies that the loss of entropy upon HLA-B*57:01-peptide-abacavir complex formation is smaller than would be the case were abacavir to remain totally rigid, thus favouring complexation. The flexibility of abacavir may offer an explanation for its specificity toward HLA-B*57:01. As previously noted, closely related alleles such as HLA-B*57:02 (Asp114Asn; Ser116Tyr; Leu156Arg), HLA-B*57:03 (Asp114Asn; Ser116Tyr) and HLA-B*58:01 (Met45Thr; Ala46Glu; Val97Arg; Val103Leu) do not bind abacavir and thus are not activated by it [6, 10]. These alleles differ from HLA-B*57:01 at a small number of sites with bulky amino acids, mainly at positions Ala46, Val97, Ser116 and Leu156. During simulations, abacavir is observed to interact with these residues (Figure 3). As a consequence, mutations in those residues that introduce a bulkier amino acid, for example Ser116Tyr or Val97Trp, likely create steric clashes which reduce the conformational space available to abacavir when bound to these MHCs. As we have shown that abacavir influences complex stability via its effect on the shape of the binding groove, rather than through direct interactions with binding pockets, bulkier residues may destabilize the pMHC-abacavir complex by limiting these effects. Other, more specific effects are also possible, for example in HLA-B*57:02 and HLA-B*57:03 the mutation Asp114Asn is likely to lower the occupancy of this residue's H-bonds with the abacavir purinyl moiety, which would destabilize such complexes.

Concluding remarks

Analysis of HLA-B*57:01-peptide-abacavir crystal structures, which represent static molecular snapshots, does not fully provide an explanation for the strong association of abacavir hypersensitivity with HLA-B*57:01. Using MD methods, however, we highlight how abacavir alters the conformational dynamics of HLA-B*57:01-bound peptides. Specifically, we show how abacavir binding can stabilize the HLA-B*57:01-peptide complexes via alteration of the conformations and flexibilities of bound peptides, via changes to the shape of the binding groove. The characterization of conformational dynamics is an important addition to crystallographic studies, that not only offer insights into abacavir-induced hypersensitivity, but may accelerate the development of safer and more effective antiretroviral drugs for the treatment and prevention of HIV.

Materials and Methods

Computational resources

Calculations, modeling and simulations were performed on ORCHARD (800 core x86 cluster, Monash University) and MERRI (x86 cluster, Victorian Life Sciences Computation Initiative, Melbourne, Australia).

Systems preparation

The coordinates for starting structures of pMHC complexes with abacavir were taken from PDB codes 3UPR [7], 3VRI and 3VRJ [6], which contain bound-peptides HSITYLLPV (pep-V), RVAQLEQVYI (RVAQ), and LTTKLTNTNI (LTTK), respectively. For each unique pMHC complex, systems with and without abacavir were simulated. The complex structures were inserted into a periodic box such that the minimum distance between any protein atom and the box face was 2 nm. All simulated systems were then solvated in water using the TIP3P water model [18]. Following immersion in water, each system was subjected to 15,000 steps of energy minimization. The simulated systems were then gradually heated to 300 K over 0.2 ns, with the protein harmonically constrained, in the canonical ensemble (NVT) conditions. Following this, all systems were simulated with harmonic constraints gradually removed over 0.2 ns, in isothermal–isobaric ensemble (NPT) conditions.

Molecular Dynamics

Molecular Dynamics (MD) simulations were performed using NAMD v2.9 software [19] in conjunction with the ff12SB all-atom force field [20, 21]. Initial abacavir geometry was extracted from a crystal structure (PDB code 3UPR [7]), and Gaussian 09 [22] was used to optimize its conformation and calculate the molecular electrostatic potential (ESP). This was done at the HF/6−31++G* level of theory, to allow for polarisation effects. The ANTECHAMBER module of AmberTools 12 [23] was then used to generate the force field libraries by assigning RESP-fitted charges, as well as Generalized Amber Force Field (GAFF)-derived parameters and atom types [24].

All simulations were performed in the NPT ensemble. The temperature was kept constant at 300 K using Langevin damping coefficient of 0.5 fs^{-1} [25]. Pressure was maintained at a constant 1 atm using Berendsen pressure bath coupling with a time coefficient of 0.1 ps [26].

A simulation time step of 2 fs was used during simulations, and the non-bonded cut-off length was set to 1 nm. Long-range electrostatic interactions were calculated using the particle mesh Ewald [27] method with a cut-off length of 1 nm. Each simulated system was repeated twice from the same starting structure but with different starting velocities and was extended to 250 ns.

MD analyses

Root Mean Square Deviation (RMSD) and Root Mean Square Fluctuation (RMSF) analyses were performed using GROMACS v4.6.5 [28]. H-bond analysis was performed using VMD version 1.9.2 [29]. Images were rendered using PyMOL [30]. RMSD and RMSF of backbone heavy atoms with respect to their initial structure were calculated every 50ps (after performing a least-squares fit [31] to the initial structure). RMSF results were reported as the average RMSF per residue backbone throughout simulations. Two atoms were defined as having an H-bond if the distance between the donor and acceptor atoms was less than 0.35 nm and the donor-hydrogen-acceptor angle was no smaller than 150°.

Acknowledgments

This work was supported by grants from the National Health and Medical Research Council (NHMRC) and the Australian Research Council (ARC). NAB is funded by an ARC Future Fellowship (110100223). This work was supported by the Victorian Life Science Computational Initiative. The authors wish to thank Dr. Grischa Meyer for providing helpful scripts, as well as the Monash eResearch Centre.

Author Contributions

AMB and NAB designed the study. IK performed molecular dynamics simulations. IK performed analysis of the MD trajectories. IK and BTR prepared the figures. IK, JF, BTR, AMB and NAB wrote the manuscript.

Conflict of interests

The authors declare no conflict of interests.

References

1. Melroy, J. and V. Nair, *The antiviral activity, mechanism of action, clinical significance and resistance of abacavir in the treatment of pediatric AIDS.* Curr Pharm Des, 2005. **11**(29): p. 3847-52.
2. Foster, R.H. and D. Faulds, *Abacavir.* Drugs, 1998. **55**(5): p. 729-36; discussion 737-8.
3. Walsh, J.S., M.J. Reese, and L.M. Thurmond, *The metabolic activation of abacavir by human liver cytosol and expressed human alcohol dehydrogenase isozymes.* Chem Biol Interact, 2002. **142**(1-2): p. 135-54.
4. Ray, A.S., et al., *Insights into the molecular mechanism of inhibition and drug resistance for HIV-1 RT with carbovir triphosphate.* Biochemistry, 2002. **41**(16): p. 5150-62.
5. Cutrell, A.G., et al., *Updated clinical risk factor analysis of suspected hypersensitivity reactions to abacavir.* Ann Pharmacother, 2004. **38**(12): p. 2171-2.
6. Illing, P.T., et al., *Immune self-reactivity triggered by drug-modified HLA-peptide repertoire.* Nature, 2012. **486**(7404): p. 554-8.
7. Ostrov, D.A., et al., *Drug hypersensitivity caused by alteration of the MHC-presented self-peptide repertoire.* Proc Natl Acad Sci U S A, 2012. **109**(25): p. 9959-64.
8. Hetherington, S., et al., *Genetic variations in HLA-B region and hypersensitivity reactions to abacavir.* Lancet, 2002. **359**(9312): p. 1121-2.
9. Rauch, A., et al., *Prospective genetic screening decreases the incidence of abacavir hypersensitivity reactions in the Western Australian HIV cohort study.* Clin Infect Dis, 2006. **43**(1): p. 99-102.
10. Chessman, D., et al., *Human leukocyte antigen class I-restricted activation of CD8+ T cells provides the immunogenetic basis of a systemic drug hypersensitivity.* Immunity, 2008. **28**(6): p. 822-32.
11. Tangamornsuksan, W., et al., *Association of HLA-B* 5701 genotypes and abacavir-induced hypersensitivity reaction: a systematic review and meta-analysis.* Journal of Pharmacy & Pharmaceutical Sciences, 2015. **18**(1): p. 68-76.
12. Yerly, D., et al., *Structural Elements Recognized by Abacavir-Induced T Cells.* Int J Mol Sci, 2017. **18**(7).
13. Kass, I., A.M. Buckle, and N.A. Borg, *Understanding the structural dynamics of TCR-pMHC complex interactions.* Trends Immunol, 2014. **35**(12): p. 604-612.
14. Hawse, W.F., et al., *TCR Scanning of Peptide/MHC through Complementary Matching of Receptor and Ligand Molecular Flexibility.* J Immunol, 2014.
15. Krogsgaard, M., et al., *Evidence that structural rearrangements and/or flexibility during TCR binding can contribute to T cell activation.* Mol Cell, 2003. **12**(6): p. 1367-78.
16. Huse, M., et al., *Spatial and temporal dynamics of T cell receptor signaling with a photoactivatable agonist.* Immunity, 2007. **27**(1): p. 76-88.
17. Reboul, C.F., et al., *Epitope Flexibility and Dynamic Footprint Revealed by Molecular Dynamics of a pMHC-TCR Complex.* Plos Computational Biology, 2012. **8**: p. e1002404.
18. Jorgensen, W., et al., *Comparison of simple potential functions for simulating liquid water.* Journal of Chemical Physics, 1983. **79**(Jorgensen, Jayaraman Chandrasekhar, Jeffry D. Madura, Roger W. Impey and Michael L. Klein): p. 926--935.

19. Phillips, J., et al., *Scalable molecular dynamics with NAMD.* Journal of Computational Chemistry, 2005. **26**: p. 1781--1802.
20. Wickstrom, L., A. Okur, and C. Simmerling, *Evaluating the Performance of the ff99SB Force Field Based on NMR Scalar Coupling Data.* Biophysical Journal, 2009. **97**: p. 853--856.
21. Hornak, V., et al., *Comparison of multiple amber force fields and development of improved protein backbone parameters.* Proteins-Structure Function and Bioinformatics, 2006. **65**: p. 712--725.
22. Frisch, M.J., et al., *Gaussian09 Revision C.01*.
23. Case, D.A., et al., *AMBER 12, University of California, San Francisco, CA*. 2012.
24. Wang, J., et al., *Development and testing of a general amber force field.* J Comput Chem, 2004. **25**(9): p. 1157-74.
25. Feller, S.E., et al., *Constant pressure molecular dynamics simulation: The Langevin piston method.* The Journal of Chemical Physics, 1995. **103**(11): p. 4613-4621.
26. BERENDSEN, H., et al., *Molecular dynamics with coupling to an external bath.* Journal of Chemical Physics, 1984. **81**: p. 3684--3690.
27. Darden, T., D. York, and L. Pedersen, *Particle mesh Ewald: An N·log(N) method for Ewald sums in large systems.* The Journal of Chemical Physics, 1993. **98**(12): p. 10089-10092.
28. Hess, B., *P-LINCS: A parallel linear constraint solver for molecular simulation.* Journal of Chemical Theory and Computation, 2008. **4**: p. 116--122.
29. Humphrey, W., A. Dalke, and K. Schulten, *VMD: visual molecular dynamics.* J Mol Graph, 1996. **14**(1): p. 33-8, 27-8.
30. Schrodinger, LLC, *The PyMOL Molecular Graphics System, Version 1.7r5*. 2010.
31. Konagurthu, A.S., et al., *MUSTANG-MR structural sieving server: applications in protein structural analysis and crystallography.* PLoS One, 2010. **5**(4): p. e10048.

Supporting Information

Table S1. Hydrogen bonds between HLA-B*57:01, peptide pep-V (PDB code 3UPR [1]) and abacavir observed over the course of the MD simulations.

HLA-B*57:01	Abacavir	Peptide **(HSITYLLPV)**	In crystal structure?	System w/o abacavir	System with abacavir
$Tyr159^{O\eta}$		$His1^{O}$	+	0.57	0.69
$Tyr171^{O\eta}$		$His1^{O}$	-	0.03	-
$Tyr7^{O\eta}$		$Ser2^{O\gamma}$	-	0.23	0.08
$Asn66^{N\delta}$		$Ser2^{O\gamma}$	-	0.21	0.41
$Tyr159^{O\eta}$		$Ser2^{O}$	-	0.02	0.46
$Tyr171^{O\eta}$		$Ser2^{O\gamma}$	-	-	0.21
$Asn66^{N\delta}$		$Ile3^{O}$	+	0.26	0.76
$Gln155^{N\varepsilon}$		$Tyr5^{O\eta}$	-	0.03	0.01
	O	$Tyr5^{O}$	-	-	0.02
$Thr73^{O\gamma}$		$Leu6^{O}$	-	0.03	0
$Gln155^{N\varepsilon}$		$Leu6^{O}$	-	0.03	-
$Thr73^{O\gamma}$		$Leu7^{O}$	-	0.29	-
$Asn77^{N\delta}$		$Leu7^{O}$	+	0.01	0.64
$Trp147^{N\varepsilon}$		$Pro8^{O}$	+	0.19	0.34
$Lys146^{N\zeta}$		$Val9^{O1/2}$	-	0.29	0.57
$Trp147^{N\varepsilon}$		$Val9^{O1/2}$	-	0.10	0.17

(-) indicates no interaction observed in simulation.
$^{O1/2}$ indicates both backbone oxygens of the C-terminus residue carboxylate group.

Table S2. Hydrogen bonds between HLA-B*57:01, peptide RVAQ (PDB code 3VRI [2]) and abacavir observed over the course of the MD simulations.

HLA-B*57:01	Abacavir	Peptide **(RVAQLENVYI)**	In crystal structure?	System w/o abacavir	System with abacavir
$Tyr159^{O\eta}$		$Arg1^{O}$	+	0.21	0.88
$Asn66^{N\delta}$		$Val2^{O}$	-	0.08	-
$Asn66^{N\delta}$		$Ala3^{O}$	-	-	0.03
$Asn66^{N\delta}$		$Gln4^{O\varepsilon}$	-	0.02	0.13
$Ser70^{O\gamma}$		$Gln4^{O\varepsilon}$	-	0.08	-
$Thr73^{O\gamma}$		$Gln4^{O\varepsilon}$	-	0.03	-
$Gln155^{N\varepsilon}$		$Gln4^{O\varepsilon}$	-	0.08	-
$Asn66^{N\delta}$		$Leu5^{O}$	-	-	0.07
$Thr73^{O\gamma}$		$Leu5^{O}$	-	0.12	-
$Asn66^{N\delta}$		$Glu6^{O\varepsilon 1/2}$	-	-	0.11
$Arg151^{N\eta 1/2}$		$Glu6^{O}$	-	0.03	-
$Gln155^{N\varepsilon}$		$Glu6^{O}$	-	0.26	0.01
	N05	$Gln7^{O}$	-	-	0.33
$Asn77^{N\delta}$		$Val8^{O}$	+	0.01	0.72
$Lys146^{N\zeta}$		$Tyr9^{O}$	-	0.04	-
	N05	$Tyr9^{O}$	-	-	0.38
$Arg83^{N\eta 1/2}$		$Ile10^{O1/2}$	-	0.13	-
$Tyr84^{O\eta}$		$Ile10^{O1/2}$	+	0.1	-
$Lys146^{N\zeta}$		$Ile10^{O1/2}$	-	0.25	0.58
$Trp147^{N\varepsilon}$		$Ile10^{O1/2}$	-	-	0.79

(-) indicates no interaction observed in simulation.
$^{O1/2}$ indicates both backbone oxygens of the C-terminus residue carboxylate group.

Table S3. Hydrogen bonds between HLA-B*57:01, peptide LTTK (PDB code 3VRJ [2]) and abacavir observed over the course of the MD simulations.

HLA-B*57:01	Abacavir	Peptide **(LTTKLTNTNI)**	In crystal structure?	System w/o abacavir	System with abacavir
Tyr159$^{O\eta}$		Leu1^{O}	+	0.01	-
Tyr7$^{O\eta}$		Thr2$^{O\gamma}$	-	0.03	-
Asn66$^{N\delta}$		Thr2$^{O\gamma}$	+	0.11	0.40
Asn66$^{N\delta}$		Thr2^{O}	-	0.02	0.05
Asn66$^{N\delta}$		Thr3^{O}	-	0.30	0.32
Tyr99$^{O\eta}$		Thr3$^{O\gamma}$	-	0.05	-
Asn66$^{N\delta}$		Lys4^{N}	-	0.02	-
	O	Leu5^{O}	-	-	0.07
Ser70$^{O\gamma}$		Thr6$^{O\gamma}$	-	-	0.03
Thr73$^{O\gamma}$		Thr6^{O}	+	0.53	0.51
Tyr84$^{O\eta}$		Thr6$^{O\gamma}$	-	0.01	-
Tyr99$^{O\eta}$		Thr6$^{O\gamma}$	-	0.04	-
Ser70$^{O\gamma}$		Asn7$^{O\delta}$	-	0.09	-
Thr73$^{O\gamma}$		Asn7$^{O\delta}$	-	0.22	0.03
	N05	Asn7$^{O\delta}$	-	-	0.04
	N05	Asn7^{O}	-	-	0.05
Asn77$^{N\delta}$		Thr8^{O}	+	-	0.29
	N05	Thr8$^{O\gamma}$	-	-	0.04
	N05	Thr8^{O}	-	-	0.02
	N06	Thr8^{O}	-	-	0.08
Gln72$^{N\varepsilon}$		Asn9$^{O\delta}$	-	0.07	-
Thr73$^{O\gamma}$		Asn9$^{O\delta}$	-	0.01	-
Asn77$^{N\delta}$		Asn9$^{O\delta}$	-	0.02	0.34
Lys146$^{N\zeta}$		Asn9^{O}	-	-	0.02
Trp147$^{N\varepsilon}$		Asn9^{O}	+	-	0.26
	N05	Asn9^{O}	-	-	0.16
Tyr84$^{O\eta}$		Ile10$^{O1/2}$	-	-	0.03
Thr143$^{O\gamma}$		Ile10$^{O1/2}$	-	-	0.05
Lys146$^{N\zeta}$		Ile10$^{O1/2}$	-	0.41	0.59
Trp147$^{N\varepsilon}$		Ile10^{O}	-	0.01	0.44

(-) indicates no interaction observed in simulation.
$^{O1/2}$ indicates both backbone oxygens of the C-terminus residue carboxylate group.

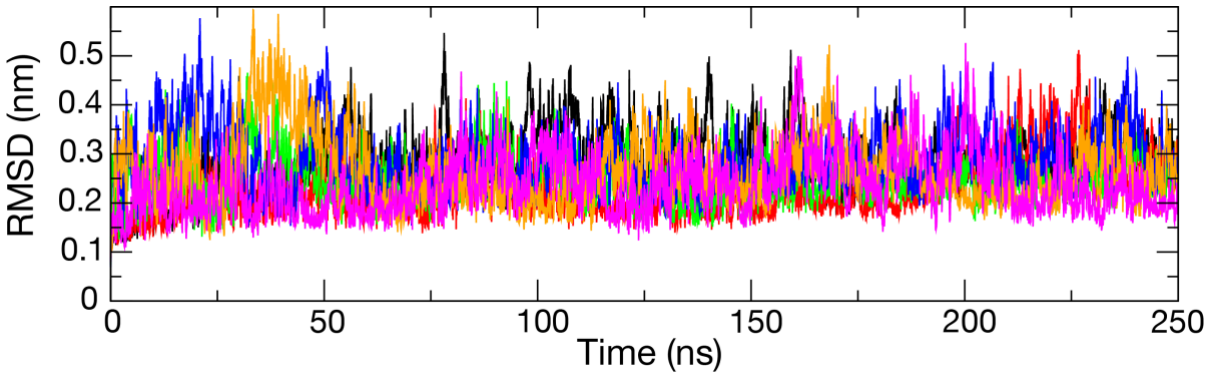

Figure S1: Representative backbone RMSDs as a function of time for MD trajectories. Representative backbone RMSDs as function of time for trajectories of PDB code 3VRI (pMHC-abacavir; black), PDB code 3VRI (pMHC, abacavir removed; red), PDB code 3VRI (pMHC-abacavir; green), PDB code 3VRI (pMHC, abacavir removed; blue), PDB code 3VRJ (pMHC-abacavir; orange) and PDB code 3VRI (pMHC, abacavir removed; pink) simulated systems. Following the initial 50 ns of simulations, the average backbone RMSDs were found to reach a plateau at 0.30 ± 0.06 nm (3UPR pMHC-abacavir), 0.24 ± 0.06 nm (3UPR pMHC, abacavir removed), 0.25 ± 0.04 nm (3VRI pMHC-abacavir), 0.28 ± 0.05 nm (3VRI pMHC, abacavir removed), 0.25 ± 0.05 nm (3VRJ pMHC-abacavir) and 0.25 ± 0.06 nm (3VRJ pMHC, abacavir removed).

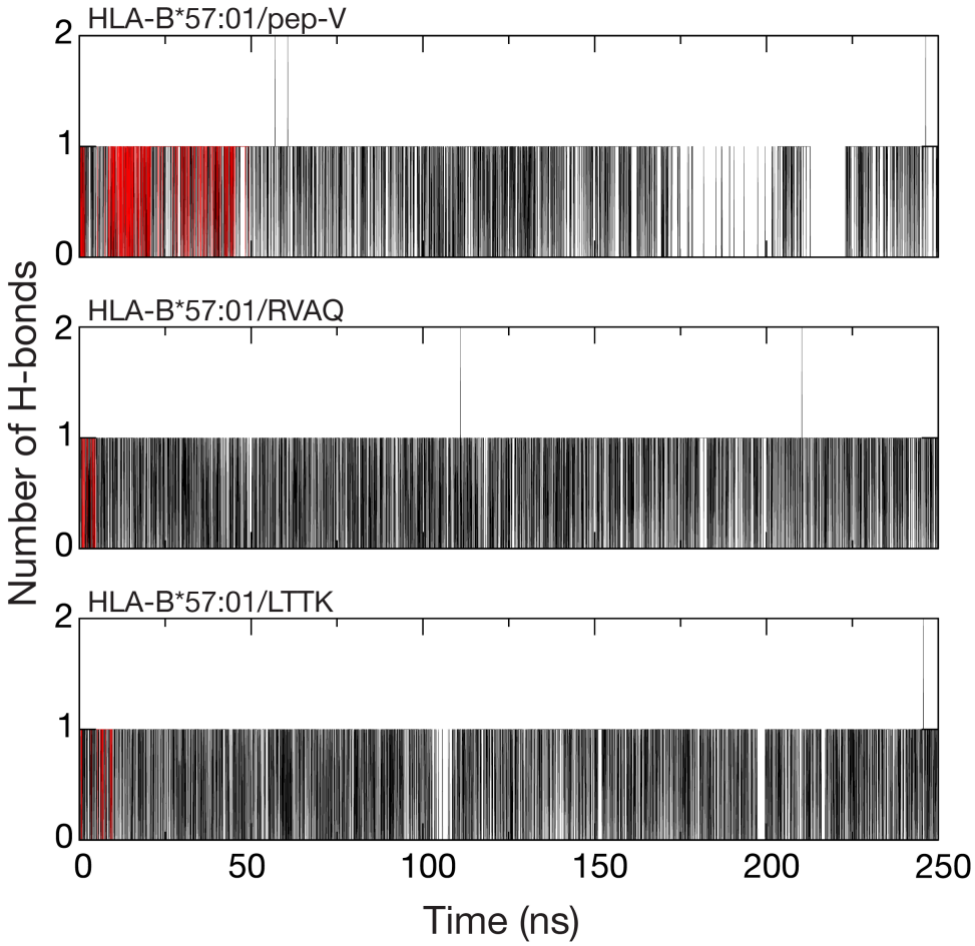

Figure S2. H-bonds between abacavir purinyl moiety and Asp114 of HLA-B*57:01 during MD simulations. Representative number of H-bonds between Asp114 and the N2 and N4 atoms of the purinyl group of abacavir (black and red, respectively) as a function of time for the three simulated systems.